Tellus SERIES A DYNAMIC METEOROLOGY AND OCEANOGRAPHY
PUBLISHED BY THE INTERNATIONAL METEOROLOGICAL INSTITUTE IN STOCKHOLM

Tellus (2008), 60A, 706–715

TELLUS

Estimation of length scales from mesoscale networks

By DANIJEL BELUŠIĆ[1*] and LARRY MAHRT[2], [1]*Department of Geophysics, Faculty of Science, University of Zagreb, 10000 Zagreb, Croatia;* [2]*COAS, Oregon State University, Corvallis, OR 97331, USA*

(Manuscript received 28 August 2007; in final form 3 March 2008)

ABSTRACT

This paper reports on the spatial scales of meandering motions using recent data from three mesoscale networks. Although the mesoscale motions extend over a wide range of scales, and time series do not reveal a spectral peak, the examination of the spatial coherence does identify a preferred spatial scale. Several independent methods reveal the same preferred spatial scale for horizontal coherence for a given network. However, the spatial scale differs by a factor of two between the different networks examined here, presumably due to the different topography and surface conditions.

The preferred spatial scale increases roughly linearly with range of time scales included in the evaluation. However, the details of this increase do not seem to be predictable, again partly due to site-specific conditions. The preferred spatial scales are of the order of a few kilometres for time scales less than an hour, but may reach tens of kilometres for time scales of several hours.

The preferred horizontal length scale determines the area over which the flow features are statistically coherent. Measurements at a single location can be considered as representative for an area comparable to or smaller than the preferred scale.

1. Introduction

The range of scales of atmospheric motion extends from large scales bounded by the planetary dimensions to scales determined by the molecular diffusion, a property of the fluid. Although the basic laws of fluid mechanics are well known, the non-linearity of the governing equations yields complex behaviour of real world systems. Despite this complexity, certain scales of motion exhibit regularity or similarity that enable their detailed study and description. Such examples include quasi-geostrophic, mid-latitude planetary scale atmospheric motions and the turbulence in the planetary boundary layer, which statistically obeys similarity relationships with stationarity and horizontal homogeneity.

However, a considerable range of scales between large-scale motions and turbulence does not seem to obey any common governing or similarity laws, at least near the surface. This is partially due to the large number of different phenomena that appear on these scales. Some of the well-defined mesoscale motions have received considerable attention, including fronts, simple gravity waves, moist convection, and thermally induced circulations. The motions on the mesoscales have, therefore, primarily been studied in terms of the well-defined phenomena. Numerous mesoscale signatures can be identified that do not have a known origin or cause, particularly in the stable boundary layer. Due to the incomplete knowledge of the variety of mesoscale processes and the complexity of their interactions, a practical generalized description of these motions has not been possible.

Spectral similarity for the mesoscales has been observed in a climatological sense in the upper troposphere (e.g. Nastrom and Gage, 1985). Several competing theories have been offered to explain the observed spectral shapes. An example is the well-known $-5/3$ mesoscale spectral slope, which can be obtained by assuming either downscale or upscale energy transfer (e.g. Lilly, 1983; Lindborg, 1999; Gage, 2004).

The situation is substantially more complicated in the planetary boundary layer (PBL) where the spectral slopes are generally poorly defined and vary with scale. This is particularly evident for weak-wind conditions where a considerable variability of wind direction is regularly observed and is difficult to explain with our current understanding of mesoscale processes.

Meandering is usually defined in terms of substantial variation of the wind direction due to emergence of the importance of mesoscale motions with weak large-scale flow (Anfossi et al., 2005). Meandering is frequently studied with respect to its effect on the horizontal dispersion of pollutants in weak-wind conditions (e.g. Gifford, 1959; Kristensen et al., 1981; Hanna, 1983; Etling, 1990; Peterson et al., 1990). The physical cause of meandering is not known, but it could be associated with internal gravity waves and various two-dimensional modes (see references in Mahrt, 2007). Unlike turbulence, meandering motions obey no known scaling relationships (Vickers and Mahrt, 2007). Meandering modes are considered to be boundary-layer motions

*Corresponding author.
e-mail: dbelusic@irb.hr
DOI: 10.1111/j.1600-0870.2008.00328.x

and often decay with height (Mahrt, 2007). However, the connection with processes above the boundary layer cannot be ruled out. Numerical mesoscale models have not been able to reproduce the mesoscale meandering (e.g. Webster and Thomson, 2005; Žagar et al., 2006), and it is not clear whether this is due to the lack of the required physics or due to strong numerical constraints (e.g. numerical diffusion) that are required for numerical stability of the models. While dispersion models pragmatically account for the meandering effect through various parametrizations (e.g. Hanna, 1990; Davies and Thomson, 1999; Anfossi et al., 2006), the physics of such motions remain unknown.

The mesoscale motions responsible for the meandering of the wind direction occur for all winds speeds (Anfossi et al., 2005), but cause significant variations of the wind direction only when the large-scale flow is weak. This is because the wind direction variability, as a first approximation, is inversely proportional to the wind speed, that is,

$$\sigma_\theta \approx \frac{\sigma_v}{V}, \tag{1}$$

where σ_θ denotes the standard deviation of mesoscale wind direction, σ_v the standard deviation of mesoscale cross-wind component and V the mean wind speed (e.g. Davies and Thomson, 1999), where cross wind is defined with respect to the large-scale flow. If σ_v is independent of V, then $\sigma_\theta \propto V^{-1}$. Indeed, the relation $\sigma_\theta \propto V^{-1}$ has been reported in several previous observational studies (e.g. Davies and Thomson, 1999, and references therein) and certain parametrizations of meandering in dispersion models are formulated in that way (e.g. Hanna, 1990; Davies and Thomson, 1999). It has also been independently shown that σ_v generally does not depend on V (Vickers and Mahrt, 2007) as also implied by the analyses of Anfossi et al. (2005). Provided that σ_v is independent of V, the horizontal dispersion due to mesoscale motions may be approximately the same for all wind speeds. This is valid if the dispersion due to mesoscale motions is governed by the relationship

$$\sigma_y = \sigma_v t, \tag{2}$$

where σ_y denotes the spread of the plume in the cross-wind direction and t the travel time. However, the cross-wind dispersion with respect to the hourly averaged wind can be regarded as being dependent on V through σ_θ, as shown by combining (1) and (2):

$$\sigma_y \approx \sigma_\theta x \approx \frac{\sigma_v}{V} x, \tag{3}$$

where x denotes the along-wind distance from the source.

For this reason we will use two measures of mesoscale variability: σ_v, or crosswind meandering velocity scale (i.e. crosswind mesovelocity scale) and σ_θ. Since meandering is due to mesoscale motions, the terms 'meandering' and 'mesoscale' will sometimes be used interchangeably. Anfossi et al. (2005) also showed that the kinetic energy of the mesoscale motions, on average, appears to be statistically independent of stability even though the physics of the mesoscale motion varies dramatically with stability.

Existing studies of meandering motions are based on Eulerian time dependence. With the exception of Hanna and Chang (1992), little work has been done on the spatial structure beyond inferences based on observed dispersion (e.g. Peterson et al., 1990). The temporal characteristics of meandering have been shown to be erratic and seemingly unpredictable. The fact that the mesoscale motions appear for all stabilities and wind speeds makes the determination of possible mechanisms more difficult. Anfossi et al. (2005) determined the correlation time scale of meandering to be about 1200 s based on the average over large number of realizations at two sites.

This paper constructs spatio-temporal statistics from recently deployed networks of atmospheric measurements. As in the time domain, spatial characteristics of meandering motions vary significantly between cases and, to this point, universal behaviour has not been identified. Therefore, the analysis is based on a large number of cases, with the goal of determining the statistical properties of spatial meandering.

2. Data

Figures 1–3 depict the three networks used in this study: Cooperative Atmosphere-Surface Exchange Study-1999 (CASES99), North Park, and Soil Moisture-Atmosphere Coupling Experiment (SMACEX) (see also Table 1). The CASES99 network was located in south central Kansas, USA, over relatively flat grass-covered terrain (Poulos et al., 2001; Mahrt and Vickers, 2002). It consists of the central 60 m tower with 8 flux measurement heights (1.5, 5, 10, 20, 30, 40, 50 and 55 m) and 6 satellite stations with flux measurements at 5 m level. The satellite stations are approximately positioned on two circles with the main

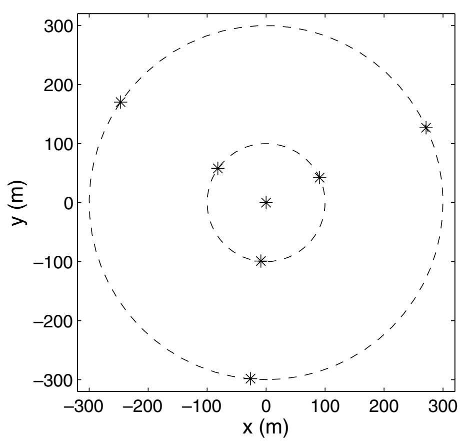

Fig. 1. Station locations in the CASES99 network. The centre coordinates, that is, the coordinates of the main tower, are 37.64855°N, −96.7361°W.

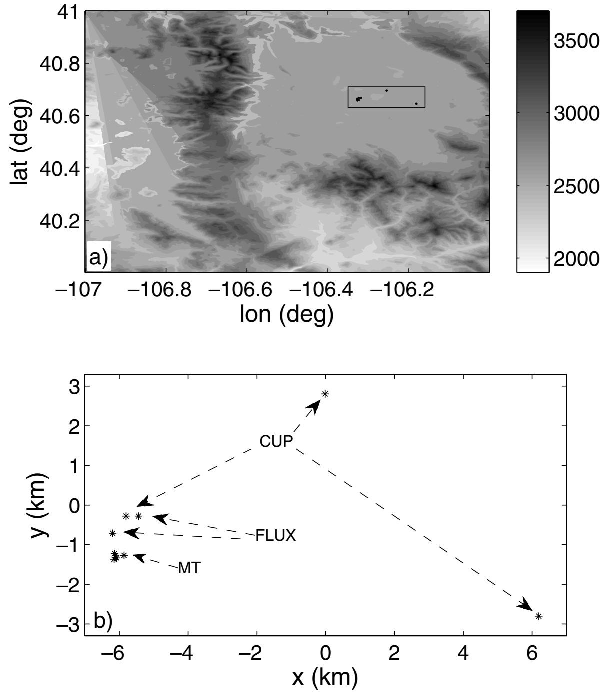

Fig. 2. (a) North Park network (black dots) and the surrounding topography. Topography contour interval is 100 m. The black rectangle outlines the network. (b) The network (rectangle from the upper panel) zoomed with station locations. MT denotes the main tower, FLUX the two additional flux measurements stations and CUP the three cup anemometer stations. Other four stations west of MT are 2-D sonics (hardly legible due to small spacing).

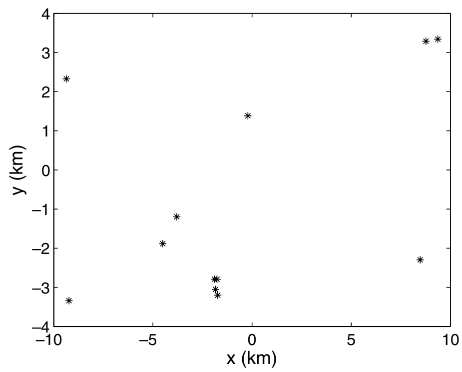

Fig. 3. Station locations in the Iowa SMACEX network. The centre coordinates are 41.9629°N, −93.6418°W.

tower at the origin and the radii of 100 and 300 m. The angle between the stations at the same radius is approximately 120°.

The North Park basin is located in northwest Colorado, USA, embedded in a complex terrain (Fig. 2a). The land use is predominantly grass with scattered brush, sometimes snow covered. The instrumentation consists of the main 30 m tower with 7 flux measurement heights (1, 2, 5, 10, 15, 20 and 30 m) (Mahrt and Vickers, 2005), 2 additional flux measurements stations at 2 m level to the north of the main tower and separated by approximately 1 km from each other and the main tower, 4 two-dimensional sonic anemometers at 1 m level with spacing less than 150 m located about 250 m west of the main tower, and three stations with cup anemometers at 2 m level, of which two are separated by more than 6 km from the main tower (Fig. 2b).

SMACEX was located in central Iowa, USA over relatively flat terrain (∼10 m height difference over 10 km), over soybeans and corn (Kustas et al., 2004). The heights of anemometers were 2 m above ground over a soybean field and 4 m above ground over a corn field, thus trying to maintain a constant height above the vegetation.

The shapes and sizes of the three networks differ significantly. While the CASES99 network resembles a regular-shaped 3-point star over a domain of 600 m across, North Park and SMACEX are significantly larger but irregularly shaped. North Park has the large gap between the closely spaced stations (spacing <1.5 km), and the two distant ones (separation > 6 km). Also, the heights of anemometers in North Park vary between 1 and 2 m. We did not attempt to correct for height-dependence, but note that we are computing spatial correlation coefficients, which are expected to be less dependent on height compared to dimensional quantities.

3. Horizontal spatial scales

The spatial (temporal) autocorrelation function and its integral over all space (time) lags, provide a measure of the governing spatial (time) scales. In practice, this integral is usually evaluated up to the first zero of the autocorrelation function (e.g. Lenschow and Stankov, 1986). This integral scale measures the distance (time) over which the signal is correlated (e.g. Sorbjan, 1989). Computed from atmospheric data, the integral scale corresponds to a statistical measure without strict formal support in that the actual flow is a complex superposition of different motions on different scales and the flow is always heterogeneous (non-stationary) to some degree.

The spatial structure of the flow can be obtained from aircraft measurements, though the quantity of data is normally small compared to in situ observations. As a result of these limitations, horizontal structure near the surface is often inferred from temporal information using Taylor's hypothesis. The latter is generally not valid for mesoscale motions in the boundary layer (e.g. Nakamura and Mahrt, 2005).

Here, we determine the spatial structure directly from the networks of data. Several different approaches for alternative estimation of the length scale are now presented. In order to use data from all of the networks in the same way, the mesoscale variation of a variable is defined as the deviation of ten-minute averages (subrecord averages) from its hourly average (record average). Ten-minute subrecord averages are chosen because they correspond to the slowest instrument sampling rate amongst all the networks (see Table 1). The coordinate system is not rotated into

Table 1. Domain size, smallest separation distance ($d_{\min}$), slowest sampling rate amongst the different instruments in the network, and the measurement period for each network

	Size (km)	$d_{\min}$ (km)	$f_{\min}$(Hz)/$T_{\max}$(min)	Period
CASES99	0.6	0.1	20 Hz	01–31/10/1999
North Park	12.6	0.06	10 min	01/12/2002–31/03/2003
SMACEX	19.8	0.13	20 Hz	20/06–09/07/2002

the direction of the large-scale flow for two reasons. First, for 1 h averages, the horizontal structure of the mesoscale motion did not depend systematically on the direction of the large-scale flow, consistent with Hanna and Chang (1992). Mesoscale motions are less influenced by the wind direction than turbulence. Second, the meaning of the mean wind direction over a network may become ambiguous, particularly for larger networks and weaker winds where the wind direction varies considerably across the network.

3.1. Correlation length scale

The first determination of the horizontal length scale is based on the dependence of the two-point correlation coefficient on the separation distance between stations of a network. For brevity, we define the 'composite' two-point correlation coefficient r_{uv} as the mean of the two-point correlation coefficients for the two wind components (r_u and r_v), i.e. $r_{uv} = (r_u + r_v)/2$, where:

$$r_\varphi = \frac{\sum_{n=1}^{N} (\varphi_{in} - \bar{\varphi}_i)(\varphi_{jn} - \bar{\varphi}_j)}{\sqrt{\sum_{n=1}^{N} (\varphi_{in} - \bar{\varphi}_i)^2 \sum_{n=1}^{N} (\varphi_{jn} - \bar{\varphi}_j)^2}}, \tag{4}$$

r_φ is the two-point correlation coefficient between stations i and j, φ represents the u or v wind component, n is the time index, N is the record length and the overbar denotes the time average over the record length (nominally 1 h). The results based on r_{uv} are qualitatively similar to those based separately on component two-point correlations, r_u and r_v. However, for a few cases, the correlation coefficients for the two wind components are significantly different, as discussed in the next section. The data are well fitted by the two-scale exponential function (e.g. Haramina and Tilgner, 2006):

$$R(x) = ae^{-bx} + (1 - a)e^{-cx}, \tag{5}$$

where $R(x)$ is the least-squares fit to the observed correlation coefficients, x is the separation distance between stations, and a, b and c are coefficients. The correlation length scale, determined from $R(x)$ under the assumption that it represents a good fit to the data, is:

$$L = \int_0^\infty \frac{R(x)}{R(0)} \mathrm{d}x. \tag{6}$$

Figure 4 depicts the dependence of r_{uv} on separation distance for the three networks. Each point represents the value of r_{uv} averaged over all records for each combination of two stations. This correlation length scale shows different values for different networks. The correlation length scales for North Park and SMACEX are 2.7 and 6.6 km, respectively (see also Table 2).

Figure 4 also reveals the inadequacies of current networks. The correlation coefficient for the small CASES99 network does not reach the e-folding distance and hence cannot be used for determination of the length scale without questionable extrapolation. CASES99 is too small for our intentions, and the rest of this study focuses on the North Park and Iowa SMACEX data. The North Park domain is sufficiently large but suffers from a significant gap in separation distances between 1.5 and 6 km. Unfortunately, these scales seem to be particularly important for assessing the horizontal length scale of the mesoscale features. The Iowa SMACEX network has a smaller gap between 1 and 2 km and is a more homogeneous setting than the North Park site, but contains only three weeks of data.

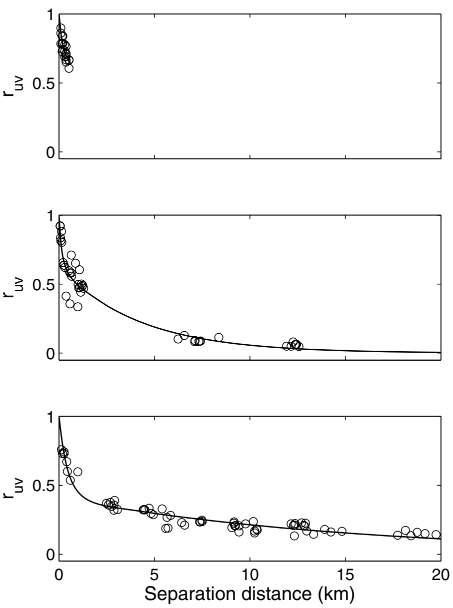

Fig. 4. Composite correlation coefficient versus separation distance between stations for the CASES99 (top), North Park (middle) and Iowa SMACEX (bottom) networks (circles). The line denotes the two-scale exponential fit to the data.

Table 2. Correlation length scales (km) for the North Park and SMACEX networks for different stabilities and wind speeds, for u and v wind components, and u–v combined

	North Park			SMACEX		
	u	v	uv	u	v	uv
All	2.4	3.1	2.7	8.0	5.3	6.6
Stable	2.3	2.7	2.4	11.2	6.3	8.0
Unstable	3.0	3.9	3.4	5.3	5.5	5.2
Weak winds	1.9	3.0	2.4	9.2	4.6	6.4
Strong winds	2.6	3.1	2.8	4.9	13.6	6.7

Stable and unstable conditions are defined in terms of the negative and positive heat flux, respectively. Weak winds are defined as $V < 1.5$ m s^{-1}, and 'stronger' winds as $V > 3$ m s^{-1}.

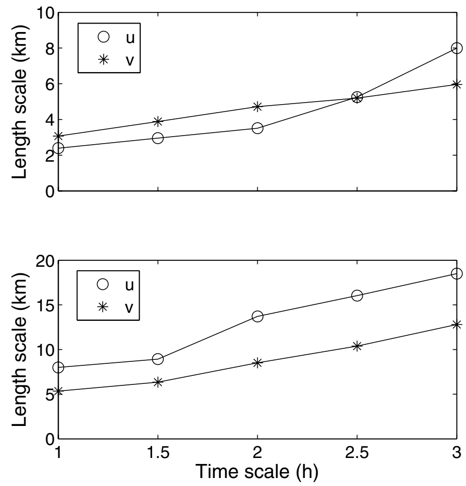

Fig. 5. Correlation length scale as a function of the record averaging time for North Park (top panel) and Iowa SMACEX (bottom).

Table 2 shows that the correlation length scale is similar for all conditions and for both wind components for the North Park network. However, the correlation length is significantly different for u and v components for the SMACEX domain for unknown reasons. The difference in L between the networks may partly be attributable to the surrounding terrain and surface features. Vickers and Mahrt (2007) found that σ_v is larger for complex terrain and forested sites, consistent with Moore et al. (1988) and Chimonas (1999). Recall that North Park is surrounded by mountains, while the CASES99 and Iowa SMACEX are located over flatter terrain. The larger σ_v for North Park, which does not lead to a corresponding increase of covariance between stations, may partly explain the stronger decorrelation and consequently the smaller correlation length scale.

Estimation of the standard error of the length scale is not possible since the length scale is determined from the fitted dependence of the correlation coefficients on separation distance. The standard error of the correlation coefficients cannot be formally computed because the records presumably represent different flow regimes and we are not selecting samples (realizations) from a homogeneous population. However, the ratio $\sigma_r/\sqrt{N_r}$ can be used as a measure of variability, where σ_r denotes the standard deviation of the correlation coefficient for a fixed separation distance and N_r is the number of samples. This ratio does not exceed 5×10^{-3}.

3.1.1. Temporal versus spatial scales. The choice of the 1-h record averaging time is arbitrary. As expected, the correlation length increases with increasing record averaging time for the North Park and SMACEX data sets (Fig. 5) (similar to Moron et al., 2007). That is, larger record length includes a larger range of mesoscale motions within the averaging window. The differences between the correlation scales determined from u and v increase with increasing record length for the SMACEX network, while there is no systematic dependence on record averaging time for North Park network.

The 10-min subrecord averaging of the original data normally filters out all of the turbulence for stable conditions, but can pass some turbulence for unstable conditions. Ten-min subrecord averaging removes some mesoscale motions on the smallest time scales for stable conditions. Decreasing the subrecord averaging to 1 min significantly reduces the correlation length (Table 3). Motions between 1- and 10-min time scales reduce the coherence between the stations, and shift the correlation length to smaller scales. The correlation length is unavoidably influenced by choice of averaging time since mesoscale motions extend over a wide range of scales.

3.2. Angle between vectors

The angle between the wind vectors at two different stations of a network is also dependent on the separation distance. The angle is calculated in the usual way, using the dot product between two vectors:

$$\cos\theta_{ij} = \frac{\mathbf{V}_i \cdot \mathbf{V}_j}{|\mathbf{V}_i||\mathbf{V}_j|}, \tag{7}$$

where $\mathbf{V}_i$ and $\mathbf{V}_j$ denote 10-min averaged wind vectors at two different stations. Since θ_{ij} is in the interval $[0, \pi]$, that is, it is

Table 3. As in Table 2, except for the SMACEX 1-min data

	u	v	uv
All	4.3	3.0	3.5
Stable	6.9	4.0	5.1
Unstable	1.9	2.1	2.0
Weak winds	5.9	3.2	4.3
Strong winds	1.6	3.7	2.2

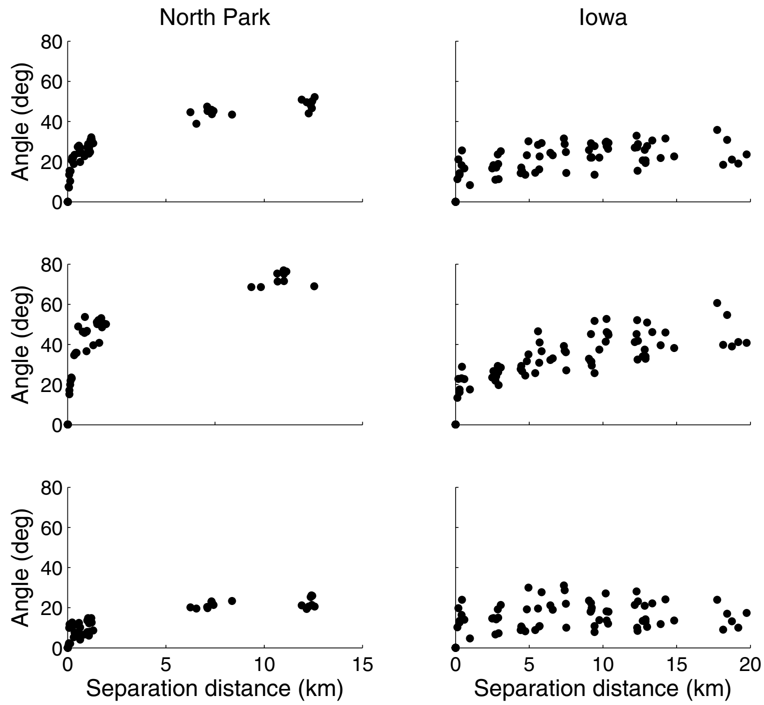

Fig. 6. Angle between two wind vectors as a function of separation distance for the North Park (left-hand panels) and Iowa SMACEX data (right-hand panels). Mean over all records (top), over weak winds ($V <$ 1.5 m s^{-1}; middle), and over strong winds ($V >$ 3 m s^{-1}; bottom).

always positive, the mean of θ_{ij} taken over all records describes the systematic variation of wind direction between two stations.

For North Park, the dependence of θ_{ij} on the separation distance (Fig. 6) is similar to that obtained above for other parameters. If the spatial scale is defined as the distance where the increase of θ_{ij} with separation distance levels off, which is about 2 km, then it again seems to be consistent with correlation lengths defined above. On the other hand, the scale cannot be determined in this way for the Iowa SMACEX data because the levelling off point is not obvious (Fig. 6) and the scatter seems too large to define a length scale by fitting the scale dependence of eq. (7).

For weak winds, θ_{ij} is significantly larger than for stronger winds. This is valid for both networks and is consistent with the fact that the mean value of θ_{ij} represents a measure of spatial variability of wind direction, which tends to increase with decreasing wind speed. Compared to the North Park data, the SMACEX data generally yields smaller values of θ_{ij}, which is consistent with smaller values of σ_v for SMACEX, apparently due to the more homogeneous terrain in SMACEX (Mahrt, 2007).

3.3. *Spatial-mean removal (SMR) technique*

The above correlation length scale is defined in terms of the time correlation between different stations. The current spatial networks do not allow for construction of autocorrelation based on spatial lags, because of too few stations. Additional difficulties in interpreting the value of the correlation length scale result from its dependence on the finite size of the data series (spatial or temporal) and the data sampling rate (or subrecord length) (Fig. 7). In the hypothetical case where the principal coherence stems from a time scale significantly larger than the record size (nominally one hour), then the determined length scale will be influenced by the averaging time. The correlation length scale determined from the two-point correlation, for a fixed separation distance, increases with increasing time (record size) over which the correlation is evaluated (Section 3.1). Similarly, reducing the subrecord averaging time (nominally 10 min) emphasizes smaller-scale motions and shifts the correlation length to smaller scales.

The spatial-mean removal technique subtracts the spatial mean for the domain from each station before computing two-point correlation coefficients. Motions on scales much larger than the domain size influence the original two-point correlations partly through the time dependence of the spatial trend across the network. Removal of the time dependent spatial mean, removes this time dependence.

A measure of the scale dependence is examined by artificially reducing the domain size. The largest spatial scale L captured by each artificial domain size S is roughly predicted as $L = 2S$ (see the Appendix). As a measure of the correlation coefficient for a given artificial domain size, we chose the maximum correlation coefficient between the different combinations of stations, for each artificial network size, which normally (but not always) equals the correlation coefficient at the smallest separation distance. Removing the spatial mean for different domain sizes leads to different resulting time series at each station and,

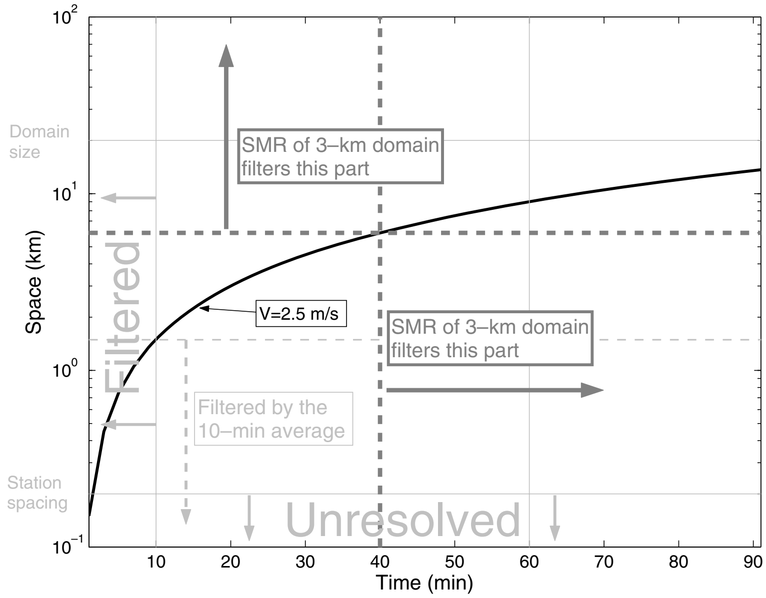

Fig. 7. Space and time scales related to the calculation of the correlation length scale and the SMR technique. In this example, the network size is 3 km, the subrecord averaging time is 10 min, and the record size is 1 h. The relation between space and time scales is illustrated for a wind speed of 2.5 m s^{-1}. The SMR regimes are thick dashed.

therefore, changes the correlations between stations even for the smallest separation distance.

In this approach, the different record and subrecord averaging time do not affect the estimated length scale, since the filtering procedure that actually determines the scale is a spatial average. Theoretically, this approach can identify multiple dominant spatial scales, which did not occur with the present data. The disadvantage is that the SMR technique is not very precise, so the results should be treated as a first approximation.

3.3.1. The SMR procedure. To summarize the SMR procedure, first remove the network spatial mean at each time step from each station:

$$\varphi_{in}^{(S)} = \varphi_{in} - [\varphi_n]_S,$$

and calculate correlation coefficients between the stations:

$$r_{\varphi}^{(S)} = \frac{\sum_{n=1}^{N}\left(\varphi_{in}^{(S)} - \overline{\varphi_i^{(S)}}\right)\left(\varphi_{jn}^{(S)} - \overline{\varphi_j^{(S)}}\right)}{\sqrt{\sum_{n=1}^{N}\left(\varphi_{in}^{(S)} - \overline{\varphi_i^{(S)}}\right)^2 \sum_{n=1}^{N}\left(\varphi_{jn}^{(S)} - \overline{\varphi_j^{(S)}}\right)^2}}, \quad (8)$$

where $r_{\varphi}^{(S)}$ is the SMR correlation coefficient between stations i and j for the artificial network size S, $[]_S$ denotes the spatial average over the network of size S, and all other symbols are as in eq. (4).

Choose a parameter that will measure the dependence on the network size, say the maximum correlation coefficient amongst the possible two station combinations. This will generally be the two stations that are closest to each other. Next, remove the most distant station of the network from the dataset, determine the new size of the network and repeat the above process of high-pass filtering (removing the mean). This may be repeated until only the most closely spaced stations remain. When a single abrupt change of the value of the chosen parameter occurs within the reduced network domain, the SMR scale is determined as twice the reduced network size (see the Appendix). Note that the absolute value of the chosen parameter is not important—it is only the relative change of value at different scales that matters.

3.3.2. Application to the data. For brevity, the following is posed in terms of the combined correlation coefficient r_{uv}. This choice does not qualitatively influence the final results. Using the Iowa SMACEX network as an example, the dependence of the correlation coefficient from data (with removed spatial mean) on the separation distance reveals smaller correlation coefficients (Fig 8a) compared to retaining the time-dependent spatial mean (Fig. 4). Much of the correlation between stations is due to the time dependence of the spatial mean. As the network size is artificially reduced and only smaller and smaller spatial scales remain after removing the spatial mean, the correlation coefficient decreases (Fig. 8b). Figures 8b and c show the dependence of the maximum correlation coefficient on the reduced size of the network for the North Park and SMACEX networks. The maximum correlation coefficient levels off with increasing network size at about 1.3 km for the North Park network and 3 km for the SMACEX network. Thus, the corresponding SMR length scales are approximately 2.6 km for North Park and 6 km for SMACEX (see Appendix), which is very close to the values obtained for the two-point correlation length scales at 1-h record averaging time (Table 2).

The dependence of the length scale on the record and subrecord averaging time is shown for SMACEX in Fig. 9. While

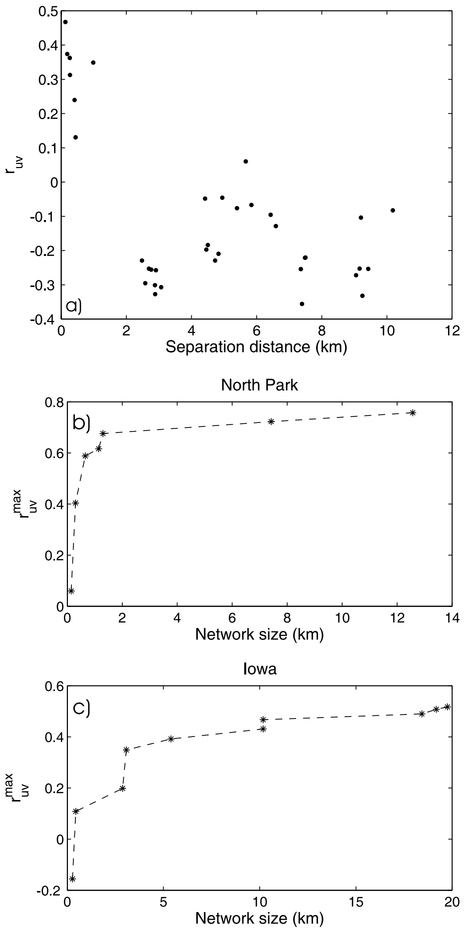

Fig. 8. (a) r_{uv} from spatial-mean removed data as a function of separation distance for the Iowa SMACEX network with a reduced size of 10 km. Maximum r_{uv} versus reduced network size for (b) North Park and (c) Iowa SMACEX.

the values of the correlation coefficient are different for different combinations of averaging, particularly for different subrecord averages, the length scale remains approximately the same, suggesting a degree of robustness.

Figure 10 shows the correlation coefficient for SMACEX between mesovelocity scales determined from the spatial domain:

$$MV^{(S)} = \sqrt{\left(\overline{\sigma_u^{(S)}}\right)^2 + \left(\overline{\sigma_v^{(S)}}\right)^2}, \tag{9}$$

where

$$\sigma_\varphi^{(S)} = \sqrt{\frac{1}{N_S}\sum_{k=1}^{N_S} \varphi_k - [\varphi]_S^2}, \tag{10}$$

and from the temporal domain:

$$MV = \sqrt{([\sigma_u]_S)^2 + ([\sigma_v]_S)^2}, \tag{11}$$

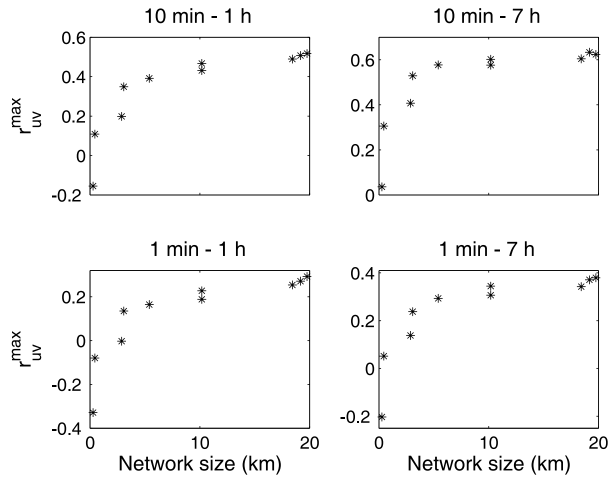

Fig. 9. Maximum r_{uv} versus network size for SMACEX. Shown are the combinations of different subrecord (1 or 10 min) and record averaging times (1 or 7 h).

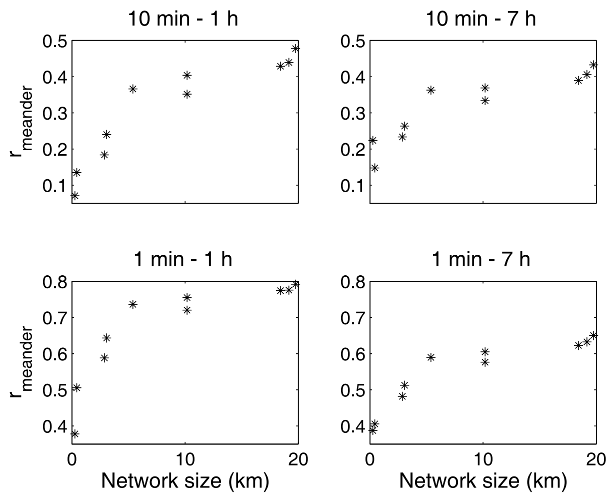

Fig. 10. As in Fig. 9, except shown is the correlation coefficient between mesovelocity scales determined from spatial and temporal domains.

where

$$\sigma_\varphi = \sqrt{\frac{1}{N}\sum_{n=1}^{N} \varphi_n - \bar{\varphi}^2}, \tag{12}$$

k is the index of a station in the network, N_S is the number of stations in the reduced network, and all other symbols are as in eq. (8). Equations (9)–(10) compute the spatial variability of the velocity components and then average such spatial variability over time. Equations (11) and (12) compute the time variance at a given point and then average such variability over space. Again, the correlation coefficient levels off approximately where the network size equals a half of the length scale (Fig. 10). This shows that the choice of the parameter that measures the decrease of the correlation is not crucial. This particular correlation coefficient

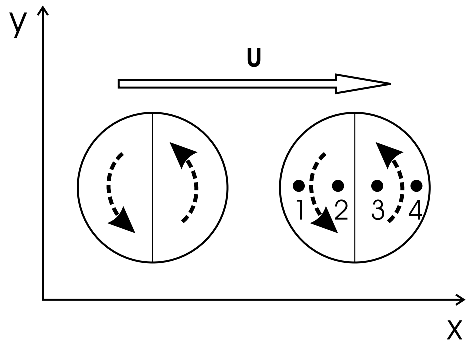

Fig. 11. A schematic explaining the definition of the SMR length scale.

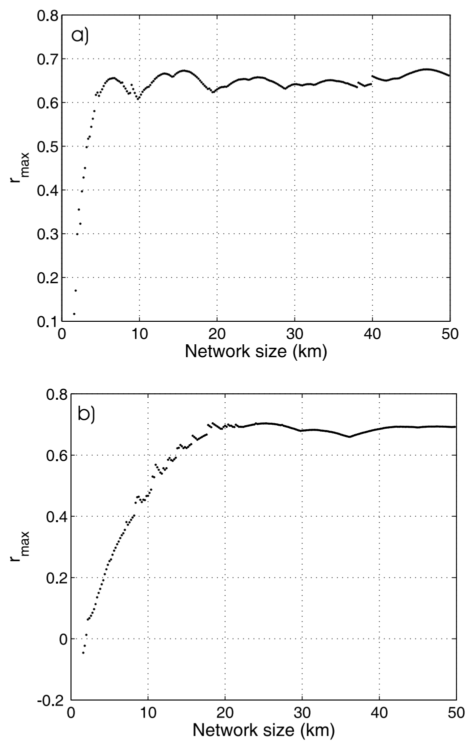

Fig. 12. Maximum correlation coefficient for the sine function with random noise versus network size. Wavelength of the sine function is (a) 10 km, and (b) 35 km.

predicts high correlation between the spatial and temporal velocity scales, which could imply stronger relation between space and time in a sense that the flow is either more homogeneous or the Taylor hypothesis is 'more' valid. For unknown reasons, the correlation is significantly higher when the subrecord averaging time is larger (1 min compared to 10 min) and is also larger for smaller record averaging time.

4. Conclusions

The above analysis of data from several different networks of surface stations indicates a definable horizontal length scale beyond which the spatial correlation is small. This spatial scale is confirmed by artificially reducing the size of the network and removing spatial means as a high-pass filtering process. Over relatively flat farmland, this horizontal length scale is greater (Iowa SMACEX, $L \sim 6.6$ km) than over a rolling basin embedded within higher mountains (North Park, $L \sim 2.7$ km). Similar numerical values of the correlation length scale are obtained from different methods, suggesting a degree of robustness. However, emergence of a robust horizontal length scale in terms of correlation functions does not correspond to a well-defined spectral maximum in wave number space.

Since the correlation between two points becomes small as the separation distance increases and approaches the correlation length, observations from a given point, such as a tower, are representative of an area that is small compared to the correlation length. The above results are applicable only in a statistical sense, that is, averaged over large number of cases. The spatial correlation varies significantly between cases.

5. Acknowledgments

Constructive discussions with Zoran Pasarić and Dean Vickers are gratefully acknowledged. We thank two anonymous reviewers for useful comments. John Preuger is acknowledged for collection of the Iowa data. This work was sponsored by DTRA through contract W911NF-06-1-0439, and the Croatian Ministry of Science, Education and Sports through project 119-1193086-1323.

6. Appendix A

A.1. Derivation of the SMR length scale

Interpretation of the SMR length scale is provided by the relation between the eddy-length scale, L, and the domain size, S. Consider a series of eddies propagating over four measuring points (Fig. 11). Also, consider the v-component of the wind vector as an example. As the eddies travel over the observational points, there is a high probability that points 1 and 4 will measure different signals. At the same time, it is highly probable that the pairs of closest points (1–2, 2–3 and 3–4) will measure similar signals. Also, assume that a small-amplitude random noise is superimposed on the eddy signal, so it does not significantly influence the correlation. Since the four points do not have the same signal due to phase shift, their mean at each moment will not resemble any of the individual point measurements. When this mean is subtracted from each point at each moment, the closest pairs of points still have similar signal behaviour and hence high correlation. When points 3 and 4 are removed from consideration, which corresponds to reducing the network size in the SMR method, the mean over the two remaining points is similar to the signals at both points. Subtraction of this mean from the two points now leaves almost only random noise at each point, and hence low correlation. Therefore, there is a transition from high to low correlation between the nearest points at roughly $S = D/2$, where D is the eddy diameter and S is again the 'network' size, so it follows that $L = D \sim 2S$.

A.2. Ideal case test

In order to evaluate the SMR technique, we constructed a wave-like sinusoidal signal with superimposed random noise. The 'network' is one-dimensional with 250 stations separated by 200 m. The period is fixed at 200 min, with specified wavelengths of 10 and 35 km. The correlation coefficients level off at about 5 and 17 km (Fig. 12), which indeed correspond to the halves of the two wavelengths, i.e. the eddy length scales.

References

Anfossi, D., Oettl, D., Degrazia, G. and Goulart, A. 2005. An analysis of sonic anemometer observations in low wind speed conditions. *Boundary-Layer Meteorol*. **114**, 179–203.

Anfossi, D., Alessandrini, S., Trini Castelli, S., Ferrero, E., Oettl, D. and co-authors. 2006. Tracer dispersion simulation in low wind speed conditions with a new 2D Langevin equation system. *Atmos. Environ*. **40**, 7234–7245.

Chimonas, G. 1999. Steps, waves and turbulence in the stably stratified planetary boundary layer. *Boundary-Layer Meteorol*. **90**, 397–421.

Davies, B. M. and Thomson, D. J. 1999. Comparisons of some parameterizations of wind direction variability with observations. *Atmos. Environ*. **33**, 4909–4917.

Etling, D. 1990. On plume meandering under stable stratification. *Atmos. Environ*. **24A**, 1979–1985.

Gage, K. S. 2004. Dynamic processes contributing to the mesoscale spectrum of atmospheric motions pp. 223–263. In: *Atmospheric Turbulence and Mesoscale Meteorology* (eds E. Fedorovich, R. Rotunno and B. Stevens). Cambridge University Press, Cambridge, UK, 280 pp.

Gifford, F. A. 1959. Statistical properties of a fluctuating plume dispersion model. *Adv. Geophys*. **6**, 117–137.

Hanna, S. R. 1983. Lateral turbulence intensity and plume meandering during stable conditions. *J. Clim. Appl. Meteorol*. **22**, 1424–1430.

Hanna, S. R. 1990. Lateral dispersion in light wind stable conditions. *Il Nuovo Cimento* **13C**, 889–894.

Hanna, S. R. and Chang, J. C. 1992. Representativeness of wind measurements on a mesoscale grid with station separations of 312 m to 10 km. *Boundary-Layer Meteorol*. **60**, 309–324.

Haramina, T. and Tilgner, A. 2006. Spatial correlation of temperature in turbulent Rayleigh-Bénard convection. *Phys. Rev. E* **74**, 066304.

Kristensen, L., Jensen, N. O. and Peterson, E. L. 1981. Lateral Dispersion of Pollutants in a Very Stable Atmosphere: The Effect of the Meandering. *Atmos. Environ*. **15**, 837–844.

Kustas, W., Li, F., Jackson, J., Preuger, J., MacPherson, J. and co-authors. 2004. Effects of remote sensing pixel resolution on modeled energy flux variability of croplands in Iowa. *Remote Sens. Environ*. **92**, 535–547.

Lenschow, D. H. and Stankov, B. B. 1986. Length scales in the convective boundary layer. *J. Atmos. Sci*. **43**, 1198–1209.

Lilly, D. K. 1983. Stratified turbulence and the mesoscale variability of the atmosphere. *J. Atmos. Sci*. **40**, 749–761.

Lindborg, E. 1999. Can the atmospheric kinetic energy spectrum be explained by two-dimensional turbulence? *J. Fluid Mech*. **388**, 259–288.

Mahrt, L. 2007. Weak-wind mesoscale meandering in the nocturnal boundary layer. *Environ. Fluid Mech*. **7**, 331–347.

Mahrt, L. and Vickers, D. 2002. Contrasting vertical structures of nocturnal boundary layers. *Boundary-Layer Meteorol*. **105**, 351–363.

Mahrt, L. and Vickers, D. 2005. Boundary-layer adjustment over small-scale changes of surface heat flux. *Boundary-Layer Meteorol*. **116**, 313–330.

Moore, G. E., Milich, L. B. and Liu, M. K. 1988. Plume behaviors observed using lidar and SF6 tracer at a flat and hilly site. *Atmos. Environ*. **22**, 1673–1688.

Moron, V., Robertson, A. W., Ward, M. N. and Camberlin, P. 2007. Spatial coherence of tropical rainfall at the regional scale. *J. Clim*. **20**, 5244–5263.

Nakamura, R. and Mahrt, L. 2005. A study of intermittent turbulence with CASES-99 tower measurements. *Boundary-Layer Meteorol*. **114**, 367–387.

Nastrom, G. D. and Gage, K. S. 1985. A climatology of atmospheric wavenumber spectra of wind and temperature observed by commercial aircraft. *J. Atmos. Sci*. **42**, 950–960.

Peterson, H., Lamb, B. and Stock, D. 1990. Interpretation of measured tracer concentration fluctuations using a sinusoidal meandering plume model. *J. Appl. Meteorol*. **29**, 1284–1299.

Poulos, G., Blumen, W., Fritts, D., Lundquist, J., Sun, J., and co-authors. 2001. CASES-99: A Comprehensive Investigation of the Stable Nocturnal Boundary Layer. *Bull. Am. Meteorol. Soc*. **83**, 555–581.

Sorbjan, Z. 1989. *Structure of the Atmospheric Boundary Layer*. Prentice Hall, Englewood Cliffs, New Jersey, 317 pp.

Vickers, D. and Mahrt, L. 2007. Observations of the cross-wind velocity variance in the stable boundary layer. *Environ. Fluid Mech*. **7**, 55–71.

Webster, H. N. and Thomson, D. J. 2005. Parameterising low-frequency meander in atmospheric dispersion models. In: *Proceedings of the 10th Int. Conf. on Harmonisation within Atmospheric Dispersion Modelling for Regulatory Purposes*. Crete, Greece, 594–598.

Žagar, N., Žagar, M., Cedilnik, J., Gregorič, G. and Rakovec, J. 2006. Validation of mesoscale low-level winds obtained by dynamical downscaling of ERA40 over complex terrain. *Tellus* **58A**, 445–455.